# Chapter 5
# Organic Solar Cells: A Review


**M. Benghanem and A. Almohammedi**

**Abstract** In this chapter, we present different materials, devices structures, and different processing techniques for the fabrication of organic photovoltaic (OPV) cells. The manufacturer of these types of solar cells uses a new process to get the best efficiencies with low cost by using printing techniques and photoactive layers based on polymer materials. Also, many scientific research works are presented and some illustrations about processing techniques, such as roll-to-roll techniques, for the design of OPV cells are presented in this chapter.

**Keywords** Organic PV cells · Processing techniques · Materials · Polymer solar cells · Devices

## 5.1 Introduction

Organic photovoltaic (OPV) cells are considered as the third-generation solar cells which present new material such as organic polymer and tandem solar cells. In this work, we give a brief review of OPV cells with different classifications and applications. The structure of the device is described as well as the organic material in the active layer of the device. The fabrication of OPV cells at low cost is possible using new processing techniques, such as roll-to-roll technique under. The organic solar cells present a low efficiency and short lifetimes compared to inorganic solar cells. The organic solar cells present the advantage to be flexible, thin, lightweight, and versatility. The next section is an overview of OPV cells. Then, we present the working principle and device structures of organic solar cells. We describe the type of material used in the active layer and we focus on the roll-to-roll (R2R) processing of organic PV cells. Our contribution in the field of organic solar cells is to synthesize the nanocrystals of Pb-chalcogenides and study their opt electrical properties in

M. Benghanem (✉) · A. Almohammedi
Physics Department, Faculty of Science, Islamic University, Madinah, Saudi Arabia
e-mail: benghanem_mohamed@yahoo.fr



A. Mellit and M. Benghanem (eds.), *A Practical Guide for Advanced Methods in Solar Photovoltaic Systems*, Advanced Structured Materials 128,
https://doi.org/10.1007/978-3-030-43473-1_5

combinations with low band gap polymers such as PTB7and PTB7-Th, for applications to the hybrid solar cells. Nanocrystals of Pb-chalcogenides will be synthesized by wet chemical methods, by mixing of precursors of Pb and chalcogenides (S, Se, Te) together at high temperature (200–350 °C). Synthesis of nanocrystals would be confirmed by XRD analysis. HRTEM, SEM, will be employed to know the shape, size, and morphology of synthesized nanocrystals. For optical and electrical characterization, the thin films of synthesized material will be prepared in combination with low band gap conjugated polymers (PTB7 and PTB7-Th) by spin coater and contact electrodes deposited by thermal evaporation method. The obtained results would be analyzed by Mathcad software to extract the important parameters such as mobility, charge carrier density, traps, and activation energy. Finally, solar cells device will be fabricated in bulk heterojunction device configuration and the performance of the device will be analyzed by measuring the J-V characteristics and impedance spectra under standard conditions.

## 5.2 Organic Photovoltaic (PV) Cells

Photovoltaic devices convert solar radiation directly into electricity using solar cells such as silicon solar cells with efficiencies reach the value of 25% in research [1]. The second generation of thin-film solar cells using materials such as cadmium telluride (CdTe) and copper indium gallium selenide (CIGS) give an efficiencies around 19.6% for CIGS [1]. The third-generation PV cells use organic materials or polymers. The organic solar cells are characterized by low efficiencies and short lifetimes and present the advantage to be flexible, thin, and versatility.

There are different types of solar cells using many technologies which are dye-sensitized solar cells (DSSC), small-molecule organic solar cells, and organic solar cells based on polymers.

The efficiencies of polymer solar cells reached the value of 8.3% [1]. The organic PV cells are constituted by a bulk heterojunction of polymer and derivatives of carbon fullerene. The first scientific research on organic PV cells using small-molecule heterojunction has been done [2]. Later, the first dye/dye bulk heterojunction PV has been designed [3]. Also, the first polymer-C60 heterojunction PV was fabricated in a research laboratory [4]. Many other research works have been focused on the development of organic PV cells [5–16].

Organic PV cells using polymers present the advantage to be flexible, thin, and also there is solution processing based on coating and printing techniques [17, 18] such as slot-die coating [19], screen [20], gravure [21], and inkjet printing [22] on a flexible substrate. The technology of fabrication plays an important role to reduce the production cost such as the fabrication using vacuum-free R2R process on flexible substrates [23].

The principle inconvenient with this solution processing is the low efficiency of organic PV cells compared with inorganic PV cells such as silicon solar cells. In fact, the efficiency obtained in the laboratory is about 8.3% while the efficiency of

the PV modules is around 3.5% [1]. Theoretically, the efficiency for single-junction cells reaches the value of 15% for tandem (multi-junction) solar cells [24, 25].

The lifetimes of organic PV cells are in excess of 1000 h of outdoor stability [26–29]. Actually, the research focuses on efficiency and stability for the same material constituting the organic solar cells.

## 5.3 Structures and Principles of Organic PV Cells

Organic solar cells are constituted by a bulk heterojunction structure which allows a better absorption of sunlight. The bulk heterojunction is a solution between electrons donor and acceptor. The donor is a polymer semiconductor like poly3-hexylthiophene (P3HT) and the acceptor can be polymers, semiconductor nanoparticles, metal oxides, or fullerenes such as PCBM in a photoactive layer [30].

In this section, we focus on fullerene material system based on the bulk heterojunction concept [31]. Figure 5.1 shows the bulk heterojunction in organic solar cells.

An organic solvent is mixed with soluble donor and acceptor material, and then the solution is deposited on the substrate with conductive layers. A penetrated network is obtained by micro-phase separation after the evaporation of the solvent. After absorption of light, we get a large space between donor and acceptor which allow the separation of the charge.

The transport of these charge to anode and cathode is due to the continuity of paths to the electrodes. To increase the efficiency of organic PV cells, an adequate combination of material using adequate treatment processes is necessary during the phases of fabrication of OPV cells.

Figure 5.2 describes the principle of organic solar cells which is established in four steps for bulk heterojunction (BHJ) devices [12, 32]. The four steps are exciton generation, exciton diffusion, exciton dissociation, and charge carrier transport to the electrodes in a BHJ solar cell:

1. Exciton generation: This step absorbs photon and allows the electron to be in the lowest unoccupied molecular orbital (LUMO) and the hole moves to the highest occupied molecular orbital (HOMO). This is due to the Coulomb forces forming an exciton.

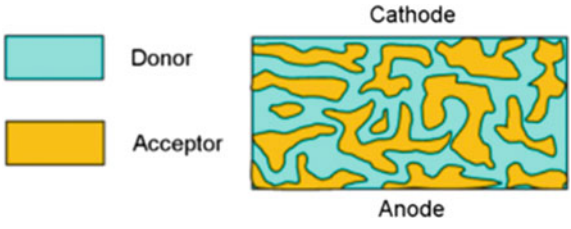


**Fig. 5.1** Layer structures in organic solar cells

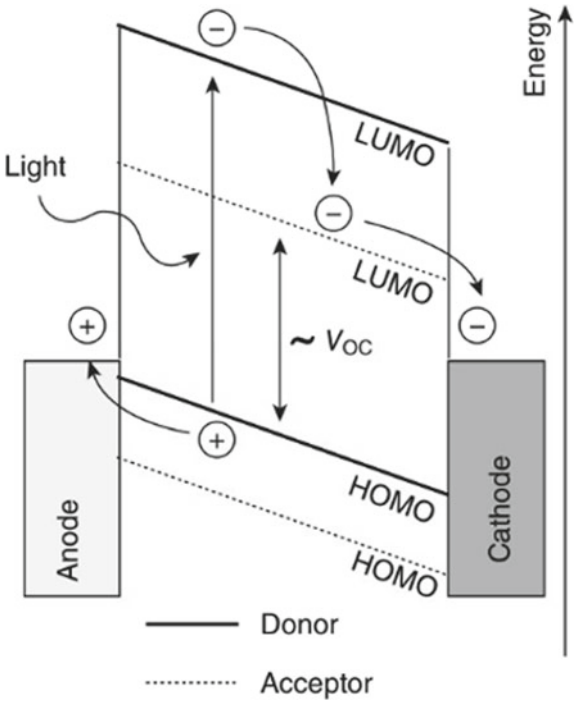


**Fig. 5.2** Band diagram of generated photocurrent

2. Exciton diffusion: The diffusion is done during the donor step to the interface of the donor and acceptor material. The concept of the bulk heterojunction of two mixed materials decreases the diffusion length and minimizes the decay rate of the exciton. The size of the two phases must be smaller than the length of the diffusion around 5–20 nm [33–36].
3. Exciton dissociation: The dissociation is done into a free electron and hole at the interface of donor and acceptor material.
4. Charge carrier transport: The charge carriers are transported via the donor and acceptor material. Negative charge are connected at the cathode, and the positive charge are collected at the anode. The generated photocurrent is due to applying a load to an external circuit. Organic materials characterized by a large absorption range can be synthesized and then influence the first step of the working principle.

Figure 5.3 presents the current density–voltage characteristics (J-V curve) for a solar cell with different factors such as the open-circuit voltage (Voc in Volt), the short-circuit current density (Jsc in mA/cm$^2$), the fill factor FF (%), and the maximum power point MPP.

The efficiency of power conversion (η) is the first essential parameter and expresses the ratio of the maximum output power ($P_M = I_{MPP} \cdot V_{MPP}$) generated by the solar cell and the input incident power of the light (Pin) on a given active area $A$:

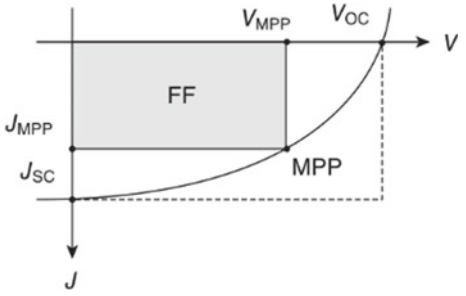


**Fig. 5.3** Characteristic J-V curve of organic PV cell

$$n = \frac{I_{MPP} \cdot V_{MPP}}{P_M \cdot A} = FF \cdot \frac{I_{SC} \cdot V_{OC}}{P_M \cdot A} = FF. \frac{J_{SC} \cdot V_{OC}}{P_M}$$

where FF is defined as:

$$FF = \frac{I_{MPP} . V_{MPP}}{I_{SC} . V_{OC}} = \frac{J_{MPP} . V_{MPP}}{J_{SC} . V_{OC}}$$

The fill factor (FF) is a parameter which can determine the performance of the produced solar cells. In general, the acceptable organic solar cells correspond to the value of FF which should be greater or equal to 65%. Two other parameters characterize the performance of solar cells which are the series resistance $R_S$ and the shunt resistance $R_{Sh}$. The series resistance represents the resistance at the interface in the layers, the conductivity of the semiconductors, and the electrodes. The shunt resistance corresponds to the defects in the layers and should be of high value.

The organic PV cells are constituted by a bulk heterojunction active layer with two electrodes as indicated in Fig. 5.4. One electrode is transparent, and generally, we use sputtering or evaporator on a transparent substrate (glass or polyethylene terephthalate) to get electrode with indium tin oxide (ITO). The last development of

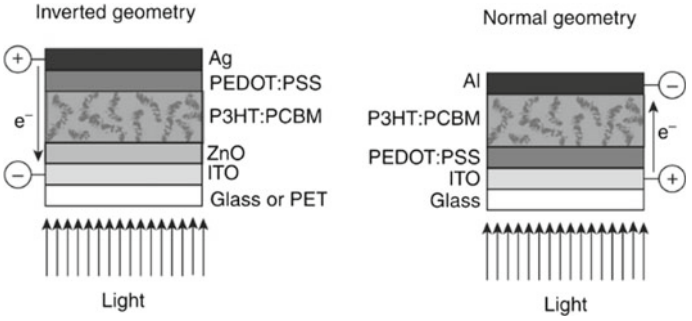


**Fig. 5.4** Organic solar cells devices with a bulk heterojunction active layer in normal and inverted geometry

**Table 5.1** The role of materials in normal and inverted geometries

| Normal geometry | | | | | |
|---|---|---|---|---|---|
| Substrate | Anode | Hole transport layer | Active layer | Electron transport layer | Cathode |
| **Glass** PET | **ITO** | **PEDOT: PSS**<br>$MoO_3$<br>$V_2O_3$ | **P3HT:PCBM** | $TiO_x$<br>ZnO | LiF/**Al**<br>LiF/Au |
| Inverted geometry | | | | | |
| Substrate | Cathode | Electron transport layer | Active layer | Electron transport layer | Anode |
| **Glass** PET<br>PEN | **ITO**<br>**Ag-solid**<br>**Al/Cr** | ZnO<br>$TiO_x$<br>$CS_2$-$CO_3$ | **P3HT:PCBM** | **PEDOT: PSS** | **Ag**<br>**Ag-**grid |

PET = Polyethylene terephthalate; PEN = Polyethylene naphthalate; ITO = indium tin oxide; PEDOT:PSS = poly(3,4-ethylenediooxythiophene):poly(styrenesulfonate); $MoO_3$ = molybdenum trioxide; $V_2O_5$ = vanadium pentoxide; P3HT = poly(3-hexylthiophene); PCBM = [6]-phenyl C61 butyric acid methyl ester fullerene derivate); $TiO_x$ = titanium oxide; nO = zinc oxide; LiF = lithium fluoride; $Cs_2CO_3$ = cesium carbonate; Al = aluminum; Au = gold; Ag = silver; and Cr = chromium

organic solar cells is to get devices with intermixed layers which are bulk heterojunction of donor and acceptor. Actually, there are two references named normal and inverted geometry, necessary to build organic PV cells in the laboratory.

The transparent ITO electrode acts as the anode in the normal geometry, whereas in the inverted structure, it acts as a cathode. Table 5.1 shows the common materials in inverted and normal geometries.

The first device structure of organic solar cells has used the normal geometry [37, 38]. The use of vacuum for evaporating the cathode electrode on the top of the active layer is considered as inconvenient of this structure.

So, to avoid this vacuum steps, the researchers opted for inverted geometry by flipping the layer stack and adding a charge transport layer which gives the best solution to the process [17].

## 5.4 Materials

The active photoconversion layer and the hole transport layer PEDOT:PSS are in principle the only organic layers in an OSC. The active layer can be polymer-based, small-molecule-based, or a hybrid organic–inorganic structure. All other layers, except the substrate, are metals or metal oxides. Here, we briefly describe the several layer materials and focus on the organic polymer-based photoactive layer at the end.

### 5.4.1 Substrate and Front Electrode

Glass or polymeric materials such as polyethylene terephthalate (PET) or polyethylene naphthalate (PEN) are the basic substrates to build on the subsequent layer structure. PET or PEN is thin and flexible and makes it the first choice in large-scale R2R processing. Indium tin oxide (ITO) is widely used as a transparent electrode on glass or PET because of its excellent properties as a hole conductor. The drawback is the price and scarcity of indium. In addition, it uses vacuum-based processes for deposition, which shows up in a huge embodied energy of more than 80% in the final device [39]. Avoiding indium and finding alternative transparent conducting electrodes is highly demanding. One promising approach without using vacuum steps is the use of printed silver grids in combination with highly conductive poly(3,4-ethylenedioxythiophene) [40]. The chemical structure of PEDOT:PSS is shown in Fig. 5.5.

### 5.4.2 Intermediate Layers (ILs)

The intermediate layer (IL) between the active layer and the electrodes acts as a charge selective conductor, either blocking electrons or holes or conducting the opposite charge and vice versa. It might also improve the alignment of the energy levels and compensate for the roughness of the underlying surface to remove some of the shunts. A myriad of different materials have been studied, but it is beyond the scope of this chapter to mention them all [41]. In normal geometries, PEDOT:PSS is the most used electron-blocking material and is dissolved or dispersed in aqueous solution. It is spin-coated on ITO, forming a thin layer with thickness of 60–100 nm and is dried at approximately 150 °C for 5–10 min.

Most of the R2R produced OSCs are based on inverted structures, where electron-conducting materials are necessary as first IL. Typical materials are $TiO_x$ or ZnO. They can easily be coated from solution-based nanoparticles or precursors of the metal oxides. An environmental side effect is obtained by using aqueous ZnO solution, and additionally, it alleviates the inflection point in the J-V curve caused by photodoping [42]. The layer thickness of the aqueous ZnO is in the range of 20 nm and needs heat treatment for 5–40 min at 140 °C to become insoluble and obtain electron-conducting characteristics.

The second IL between the active layer and back electrode acts as charge selecting layer similar to the first IL and has to have the opposite blocking characteristics than the first one. In OSCs with normal geometry, a second IL is not mandatory but materials like $TiO_x$ and ZnO improve the efficiency and act as environmental barrier, inducing stability [43–45]. At the same time, the thin oxide layer can improve the optical absorption by shifting the field distribution inside the cell. Hole conducting PEDOT:PSS has been typically used in OSCs with inverted geometry, but $MoO_3$ and $V_2O_5$ have also been reported [46]. Applying water-based PEDOT:PSS on top

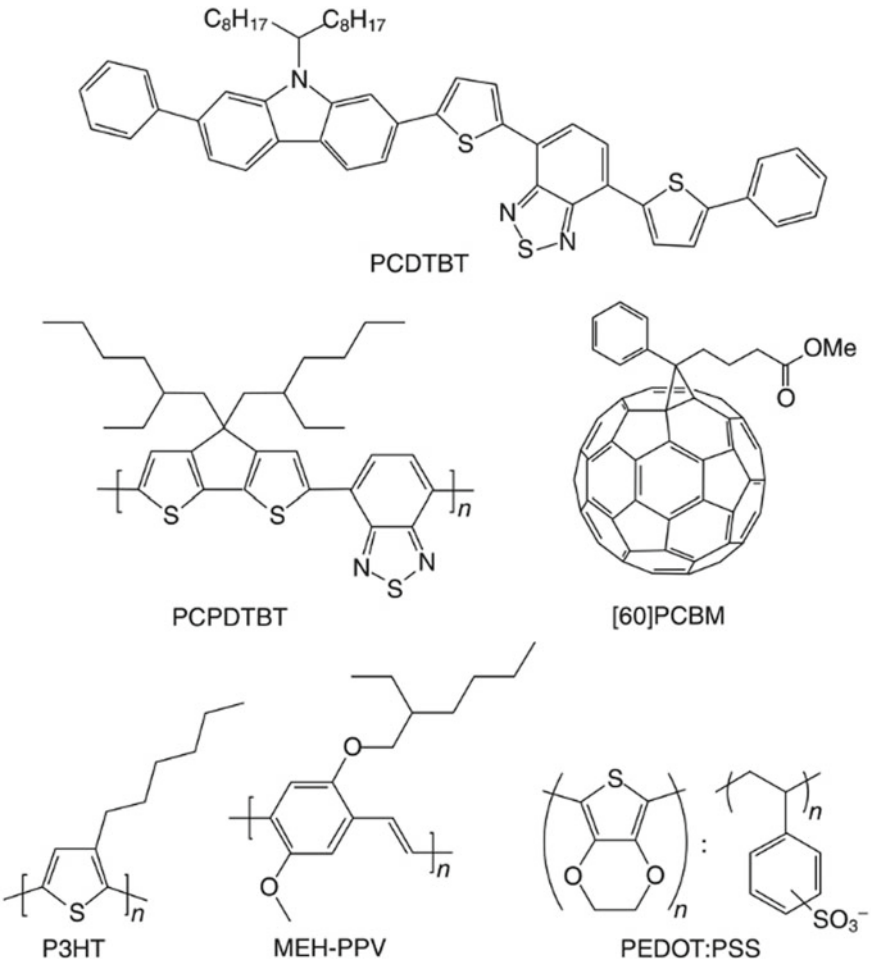


**Fig. 5.5** Chemical structure of organic material used in OSC

of a hydrophobic PCBM:PCBM film, which causes dewetting and inhomogeneous layers, is almost impossible. Therefore, a special screen-printing formulation of PEDOT:PSS diluted in isopropanol is used for R2R coating [17]. For P3HT:PCBM-based OSCs, the interface between the active layer and PEDOT:PSS was found to be the weakest [47]. Delamination and thermomechanical stresses may result in poor device performance. Annealing time and temperature increase the adhesion in this interface.

### 5.4.3 Back Electrode and Encapsulation

A metallic back electrode completes the OSC structure and acts as either anode or cathode depending on the geometry. The most commonly used electrode material is aluminum, silver, and gold, but calcium has been reported too. Aluminum is often applied with a thin layer of lithium fluoride (2–10 nm), which improves contact to the active layer. Furthermore, it protects the active layer from damage during the evaporation [48]. In normal devices, the electrode is thermally evaporated and therefore not well suited for R2R processes. Silver electrodes can be easily applied by screen printing on inverted devices. The silver paste is commercially available and easy to process, but the influence of different solvents in the ink on the active layer has to be considered [49].

Encapsulation is necessary to prevent exposure to humidity and oxygen. A barrier material with a sufficient oxygen transmission rate (OTR) of at least $10{-}3\ cm^3\ m^{-2}\ day^{-1}\ atm^{-1}$ and a water vapor transmission rate (WVTR) of at least $10{-}4\ gm^{-2}\ day^{-1}$ is required [50, 51]. Devices prepared on rigid substrate are typically encapsulated with glass or metal using epoxy. Flexible barrier foils are used for large-scale flexible encapsulation and can be applied by lamination with pressure-sensitive adhesives (PSA) [52]. Alternating layers of inorganic oxides such as SiOx and polymers in the barrier foil are used to achieve high OTR and WVTR.

### 5.4.4 Active Layer

Light absorption and charge carrier generation happen in the photoactive layer and therefore huge research efforts are being made to develop high-performance donor and acceptor materials. The main challenges are good stability, material abundance, cost efficiency, and large-scale processability, although not everything is fulfilled by one material at the moment. The following section outlines some of the more successful materials for OSCs extracted from countless reports. Table 5.2 summarizes the current state-of-the-art OSC laboratory-scale devices and shows the solar cell parameters for different materials and device structures.

The bulk heterojunction, interpenetrating network by blending donor and acceptor material, was introduced in 1995 and showed great improvements in charge separation and efficiencies [53]. They used 2-methoxy-5-(2-ethylhexyloxy)-polyphenylenevinylene (MEH-PPV) as electron donor and the soluble fullerene derivate [6]-phenyl C61 butyric acid methyl ester (PCBM) as electron acceptor in the intermixed active layer (Fig. 5.4). A bulk heterojunction active layer with material combinations of poly(3-hexylthiophene) (P3HT) (Fig. 5.4) and PCBM or PCBM is state of the art and well studied. Efficiencies are in the range of 5% [37, 38]. The mismatch of the absorption spectrum of P3HT with the solar emission spectrum

**Table 5.2** Solar cell performance parameters of state-of-the-art bulk heterojunction OSC

| Structure | $V_{OC}$ (V) | $J_{SC}$ (mA/cm$^2$) | FF (%) | PCE (%) |
|---|---|---|---|---|
| ITO/PEDOT: PSS/**P3HT**: **PCBM**/Al | 0.63 | 9.5 | 68 | 5.0 |
| ITO/PEDOT: PSS/**PCDTBT**: **PCBM**/BCP/Al | 0.91 | 11.8 | 66 | 7.1 |
| ITO/PEDOT: PSS/**PCDTBT**: **PCBM**/$TiO_x$/Al | 0.88 | 10.6 | 66 | 6.1 |
| ITO/PEDOT: PSS/**P3HT:bisPCBM**/Sm/Al | 0.72 | 9.14 | 68 | 4.5 |
| ITO/PEDOT: PSS/**PTB7**: **PCBM**/Ca/Al | 0.74 | 14.5 | 69 | 7.4 |

Active layer is highlighted in bold

limits further improvement in efficiency. P3HT has a band gap of around 1.9 eV and absorbs only wavelength below 650 nm. The photon flux reaching the surface of the Earth has a maximum of approximately 1.8 eV (700 nm), and therefore, P3HT can harvest only 22.4% of available photons [54].

A way to overcome this physical barrier is the synthesis of polymer material with low band gaps collecting as many photons as possible. The offset of the HOMO and LUMO levels between donor and acceptor becomes important as well, whereas the open-circuit voltage of the device is defined by the difference between the energy level of the HOMO in the donor and the energy level of the LUMO in the acceptor. The lowest band gap of the two materials defines the maximum current. In the case of PCBM as acceptor, the optimum band gap has to be in the range of 1.2–1.7 eV. Absorption of more photons leads to potentially higher efficiencies.

The preparation of low band gap (LBG) polymers follows the donor–acceptor approach, in which the polymer backbone has electron-rich and electron-poor domains. One of the most promising and efficient LBG polymers is poly[2,6- (4,4-bis-(2-ethylhexyl)-4H-cyclopenta[2,1-b;3,4-b′]-dithiophene)-alt-4,7-(2,1,3-benzothiadiazole)] (PCPDTBT), which is based on a benzothiadiazole unit (acceptor) and a 4,4-bis (2-ethylhexyl)-4H-cyclopenta[2,1-b;3,4-b′] dithiophene unit (donor). That band gap is around 1.46 eV. Reported power conversion efficiencies are up to 4.5% in combination with PCBM and 6.5% with PCBM [55]. High efficiencies of up to 7.1% were achieved with the LBG polymerpoly[N-9″-hepta-decanyl-2,7-carbazole-alt-5,5-(4′,7′-di-2-thienyl-2′,1′,3′-benzothiadiazole)] (PCDTBT) and [12] PCBM dissolved in dichlorobenzene and 13% dimethyl sulfoxide (Chu et al. 2011). The cell had very good characteristics with VOC of 0.91 V, JSC of 11.8 mA/cm$^2$, and a FF of 66%. Further LBG polymers are reviewed in detail [54, 56].

The active layer is processed out of a blend solution of donor and acceptor. In case of P3HT:PCBM, the optimal ratio is around 1:1 [37] with concentration of 20–40 mg/ml. The range of solvents is large, but chlorobenzene or dichlorobenzene is typically used [57]. A certain dry layer thickness is achieved after deposition of the ink and evaporation of the solvent. The theoretical maximum JSC with a 5 μm

thick active layer is calculated with 15.2 mA/cm$^2$ for an IQE value of 100%. For more realistic thicknesses of 400 nm and an IQE value of 80%, the JSC decreases to 10.2 mA/cm$^2$ [58].

Improving the efficiency of the device is done by thermal annealing the active layer. This can drastically change the structure and morphology of the material [59, 60]. P3HT can crystallize when the temperature is above the glass transition temperature. The concentration of PCBM has also an influence on the morphology upon annealing [61]. It can improve the phase separation due to PCBM cluster growth. Other possibilities to improve the morphology of the active layer are solvent vapor treatment [62] and additives in the active layer ink.

Polymers are made soluble by attaching solubilizing side chains such as alkyl groups onto the conjugated polymer backbone. They do not contribute to the light harvesting and make the material soft, which is related to the instability of OSCs [26]. After solution processing and drying, the side chains are useless and then can be removed. This interesting application can be achieved with thermocleavable materials. Thermocleavable ester groups are attached to the polymer backbone with a branched alkyl chain as solubilizing group. After heating to 200 °C, the solubilizing groups are eliminated leaving the polymer insoluble. Heterojunction devices with poly-3-(2-methyl-hexan-2-yl)-oxy-carbonylbithiophene (P3MHOCT) and C60 showed an improved stability after thermal treatment [26]. The P3MHOCT is converted to the more rigid and insoluble poly-3-carboxydithiophene (P3CT) at 200 °C, and with further heating at 300 °C, it is converted to native polythiophene (PT) (Fig. 5.6).

The cleaving is visible due to a color change from red over orange to purple-blue. OSC devices prepared with P3MHOCT:PCBM showed a large improvement in efficiency from P3MHOCT over P3CT to PT yielding at 1.5% for PT:PCBM [63]. Thermocleaving can be seen as a breakthrough in the processing of polymers and adopting this technique to other polymers offers several advantages such as only having the active components are in the final layer. Detailed information about thermocleavable polymers can be found in [13, 64, 65].

Polymer material development and new active layer concepts such as polymer–polymer solar cells, inorganic–organic hybrid solar cells, and nanostructured inorganics filled with polymer are extremely fast-moving fields of research. Tandem

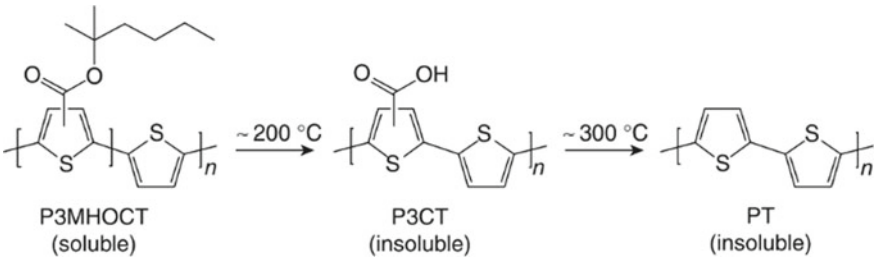


**Fig. 5.6** Preparation of OT via a thermolytic reaction

OSCs improve the cell efficiency by stacking different band gaps materials on top of each other. The challenge is not only to find good material combinations to harvest as much photons as possible. From the processing point of view, the solvents and solubility of each subsequent material must match to prevent negative interaction like dissolving.

Thermocleaving and protecting the intermediate layer can improve the development of these multi-junction solar cells. Covering all of the further technologies in this chapter is not possible and we refer the reader to extensive review reports [12, 66, 67]. For the sake of completeness, it shall be mentioned that small-molecule organic solar cells [68, 69] are another group of organic solar cells and typically fabricated by vacuum processing in the preferred p-i-n structure [70, 71], employing either exciton blocking layers, or p-doped and n-doped electron transport layers. The intrinsic active layer is either a stacked planar heterojunction or a bulk heterojunction of donor and acceptor materials. The acceptor is typically the fullerene C60. Donor materials used are polyacenes [72], oligothiophenes [73], and metal phthalocyanines as benchmark materials [69]. Copper phthalocyanine (CuPc) and zinc phthalocyanine (ZnPc) are the most studied materials.

Red-absorbing fluorinated ZnPc (F4-ZnPc) can lead to 0.1–0.15 V higher open-circuit voltage than standard ZnPc. Combined with green-absorbing dicyanovinyl-capped sexithiophene (DCV6T) in a tandem cell structure, it can lead to an absorption over the whole spectrum with efficiencies up to 5.6% [74]. Efficiency of more than 8% in a tandem structure has already been achieved [1]. A drawback of small-molecule OSCs is the energy-intensive vacuum processing. Recent developments demonstrate solution-based small-molecule solar cells [75].

Efficiency of 6.7% was achieved with 5,5′-bis{(4-(7-hexylthiophen-2-yl) thiophen-2-yl)- [1, 2, 5] thiadiazolo [3,4-c]pyridine}-3,3′-di-2-ethylhexylsilylene-2,2′-bithiophene, DTS(PTTh2)2 as donor, and PCBM as acceptor dissolved in chlorobenzene. The normal structured bulk heterojunction device still comprises an evaporated Al cathode.

## 5.5 Roll-to-Roll (R2R) Processing of Organic PV Cells

The fabrication of organic solar cells is based on coating and printing techniques. The advantages of organic solar cells consist of the low-cost and very big production of such solar cells. Table 5.3 presents the performance of P3HT: PCBM solar cells, in which the active layer is fabricated with various process technologies such as roll-to roll (R2R) processing, slot-die [17, 19, 28], gravure [21, 76], screen printing [77], and inkjet [22, 78].

The preparation of standard solar cells in the laboratory using spin coater or evaporating systems presents the inconvenience which is the small active area and the loss of material during operation of fabrication by spin coater. The produced solar cells with such technology are limited due to the limitation of size, limited photocurrent, and low open-circuit voltage under 1 volts. To increase the productivity and to get

**Table 5.3** Solar cell parameters of organic solar cells with P3HT: PCBM layers obtained by printing processes and coating

| Process (active layer) | Active area ($cm^2$) | $V_{OC}$ (V) | $I_{SC}$ (mA) | FF (%) | PCE (%) |
|---|---|---|---|---|---|
| (a) Slot-die | 4.80 | 3.62 | 6.86 | 44.00 | 2.33 |
| (b) Slot-die | 96 | 7.56 | 60.00 | 38 | 1.79 |
| (c) Slot-die | 13.2 | 6.48 | >6 | 64 | 2.20 |
| (d) Gravure | 9.65 | 3.02 | 13.91 | 44.00 | 1.92 |
| (e) Gravure | 0.045 | 0.56 | 0.22 | 45.00 | 1.21 |
| (f) Screen printing | 1.44 | 0.59 | 21.07 | 29.78 | 2.59 |
| (g) Inkjet | 0.16 | 0.57 | 1.50 | 45.00 | 2.40 |
| (h) Inkjet | 0.09 | 0.628 | 0.9612 | 55.27 | 3.71 |

more output power of solar cells, we use R2R coating and printing techniques which allow the maximum use of material without loss. In general, in this technique, we use the inverter layer structure which allows to print the silver electrode with no vacuum.

The materials used for organic solar cells are soluble as printable ink and the used transparent conductive electrode ITO are evaporated on the flexible substrate. Due to the high cost of ITO and the embodied energy in organic solar cells is greater than 80% [39], many researches focus to avoid ITO and to use instead alternative materials like highly conductive polymers [79, 80]. For R2R processing, we use the flexible substrate and transparent foils such as polyethylene terephthalate (PET) and encapsulation using flexible barrier material allowing the final device lightweight and thin.

1. Full R2R, inverted structure, module of 8 serial connected cells [17].
2. Full R2R, inverted structure, module of 16 serial connected cells, average value over 600 modules, and max. PCE 2% [19].
3. Flatbed process, 11 serial connected cells, ITO-free, Cr/Al/Cr on flexible plastic substrate, and evaporated Au grid [28].
4. Normal geometry, flatbed process, and 5 serial connected cells [21].
5. Inverted structure, flatbed process, single cell, and evaporated Au electrode [76].
6. Normal structure, flatbed process, and evaporated Al electrode [77].
7. Normal structure and evaporated Al electrode [78].
8. Normal structure and evaporated LiF/Al electrode [22].

### *5.5.1 Serial Interconnected Device Structure*

Organic solar cells module based on typical R2R consists of numerous serial interconnected single cells to get open-circuit voltages as illustrated in Fig. 5.7.

If we need 12 V in our PV system, we should connect 24 single cells with an open circuit of 0.5 V. The total photogenerated current is equal to the photogenerated

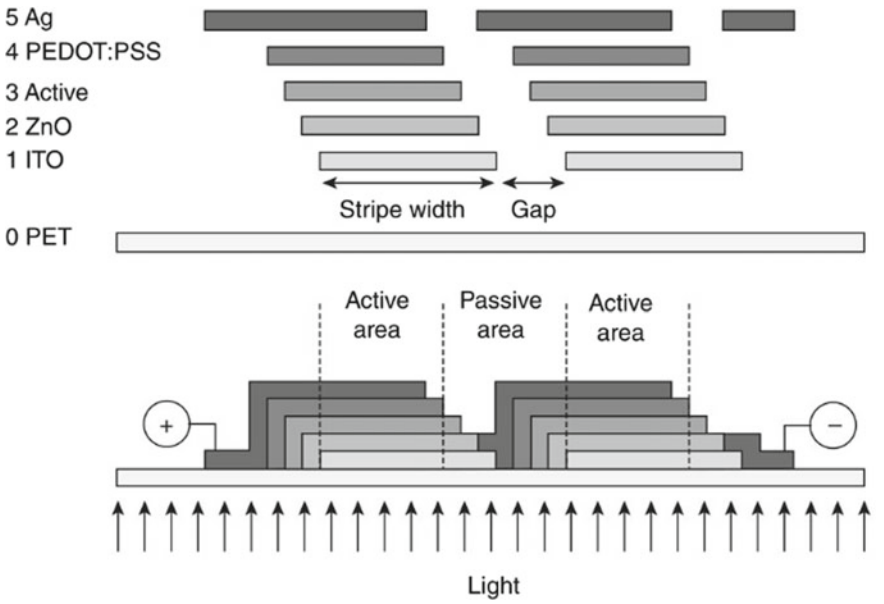


**Fig. 5.7** Serial interconnected of 2 single cells (inverted structure) (0) substrate PET, (1) ITO, (2) ZnO, (3) active layer, (4) PEDOT:PSS, and (5) Ag layer active area: generation of photocurrent

current of a single cell. This is due to the serial connection of identical solar cells which give the same short-circuit current. The production process using printing and coating allows homogeneous layer quality. During the industrial fabrication, we avoid any changes by fixing the process conditions in order to get similarity in the single cells. In research purposes, we can continuously change factors in R2R process. The conductivity of the electrode material depends on the width of the single cell, and upscaling reduces the photogenerated current.

The organic solar cells produced using R2R process have a stripe width of 4–20 mm for ITO (electrode material) and calculations of the size dependence [81]. Also, the small cell width decreases the relative active area of the module and some deposited material does not produce photocurrent. Many research [80, 82] focuses on monolithic design architecture with a high active to total area ratio by using highly conductive electrode material. The simplicity of manufacturing of this kind of device structure is an advantage since there is no required pattern.

### *5.5.2 Coating and Printing Processes*

We describe in this section the process related to printing and coating for fabrication of OSCs devices. In fact, due to the facilities and availability of necessary materials and polymers for solution processing, it will be easy to transfer the laboratory-scale

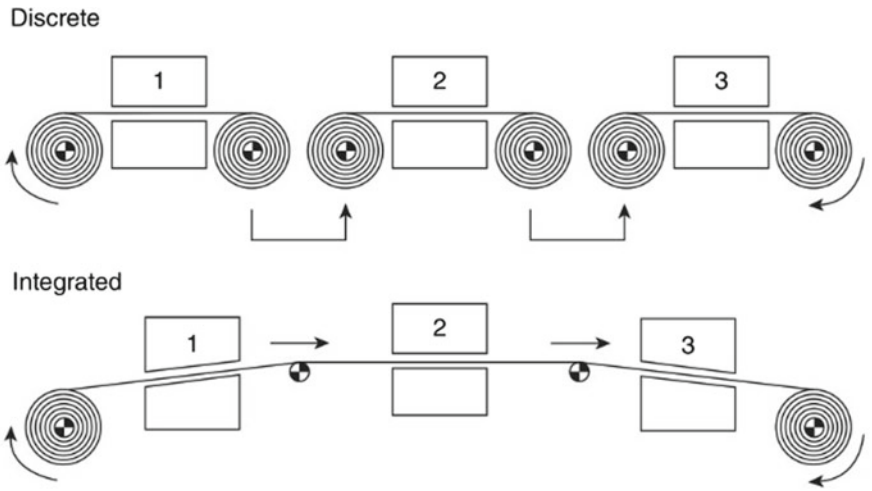


**Fig. 5.8** Comparison between integrated R2R and a discrete process

spin coating process to large scale such as R2R coating and printing processes. Additive deposition of material affects the price of the production of OSC devices. The technologies used in thin-film fabrication like photographic from industrial sectors can be suitable for the fabrication of OSCs.

The organic solar cell is based on different layers which may need various processing technologies, intermediate treatments, or different factors such as time of drying and web speed. To minimize the cost of steps in vacuum process, we prefer a structure using an inverted layer and printable electrodes. Also, it is desired to use an integrated R2R processing on a single factory line, but the different needs for each step allows discrete processing steps for the multi-layer OSC, as illustrated in Fig. 5.8. An optimization and best control represent an advantage of single-step processing. A total production can be stopped by any failure during the different steps of the process. An optimization can be done on different available machines of coating and printing following the needs of manufacturing. Printing methods are adequate to R2R processing, and different technologies can be used in a plant to fulfill the fabrication requirements for all layers, inks, and process parameters.

The principal need for the thin-film layer is homogeneity without pinholes over a large area [10, 83–86].

### *5.5.3 Slot-Die Coating*

Slot-die coating provides smooth layers with homogeneous thicknesses in different directions. Figure 5.9 shows the system of coating. As it is described, the wet layer thickness is controlled by the coating speed and the flow rate of the supplied ink.

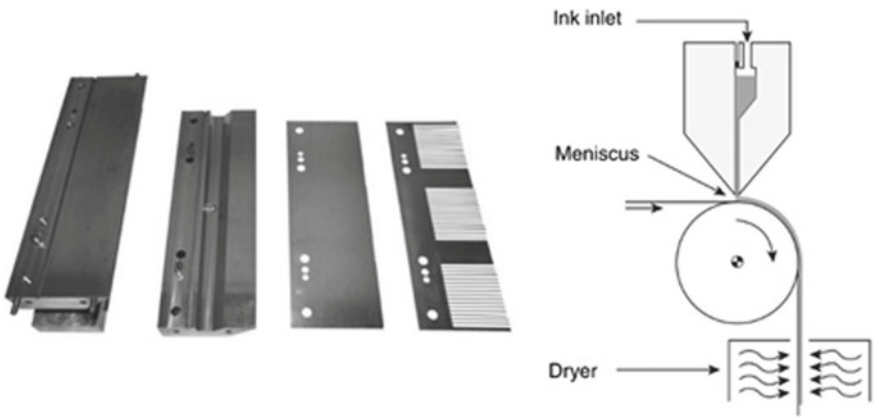


**Fig. 5.9** Slot-die coating process (right) and the disassembled head including the stripe mask (left)

The coating head is precision engineered and it is not easy to get the same pressure distribution along the coating width. Multi-layer structures of organic solar cells are produced by displacing the head perpendicular to the web direction to align the stripes of materials in each process step. By inserting the stripes masks into the head, we get the stripes, forming a stripe-wide meniscus at the outlet of the ink. The ink viscosity adjusts the thickness of the mask and is in the range of 08–210 μm. Low-viscous polymer solutions for OSCs with viscosities below 20 MPa require masks with thicknesses of 25–55 μm. Due to the different wetting behaviors of the ink, the masks should be varied. The coating head lip is never in contact with the substrate. Pre-coated is not influenced by contact pressure such as in other printing technologies.

By using syringe pumps or piston, we pump the ink into the head. Higher viscous inks above 110 mPa may require pressure vessels with flow control equipment. The total coating process including the ink tank is a closed system which is useful for solvents. The wet layer thickness is fixed by the ink and web speed. The final dry layer thickness can be calculated with the following relation:

$$d = \frac{f}{Sw} \cdot \frac{c}{\rho}$$

$d$ represents the thickness in cm, $f$ represents the ink flow rate in $cm^3$/min, $c$ is the solid concentration in the ink in $g/cm^3$, $S$ is the web speed in cm/min, $w$ is the coated width in cm, and $\rho$ represents the density of the dried ink material in $g/cm^3$.

Typical values of coating speeds for the fabrication of organic solar cell, with slot-die coating, are 0.4–2.5 m/min. This depends on the viscosity and the time of drying. The maximum drying temperature is fixed by substrate. Figure 5.10 presents a photon of slot-die coated organic solar cell modules with screen-printed silver electrodes [87]. Slot die can also be used for the coating of silver nanoparticle ink to

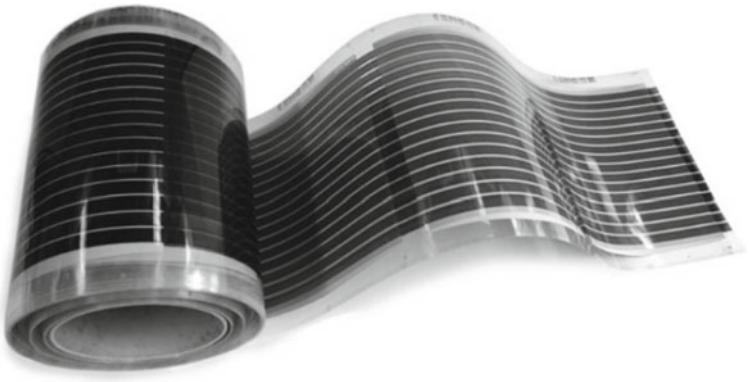

**Fig. 5.10** Flexible OSCs modules fabricated by R2R slot-die coating with screen-printed silver electrodes

form electrode layers as a substitute for ITO [20]. Nanoparticle inks can be coated through slot-die coating technology. The coating factors and the properties of the ink should be optimized to reach the best quality of layer.

To study the material compositions in the processing parameter space [87], R2R slot-die coating is used as a research tool. Figure 5.11 shows the principle of differential pumped slot-die coating using two pumps for the material screening of ink compositions. This technology allows the material screening and characterization of OSCs with very small amounts of material in a R2R process. This late presents an advantage by comparison with individual spin coating. In fact, an optimization is obtained about the material ratios like P3HT to PCBM, and best layer thicknesses are much faster.

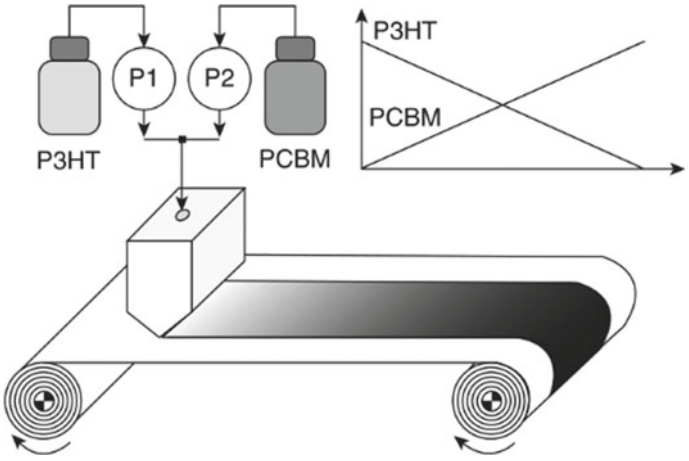


**Fig. 5.11** Differential pumped slot-die coating for material screening of ink compositions

### 5.5.4 Screen Printing

For laboratory-scale research, we can use the technique of screen printing which is low-cost process. Also, this technique is used in the industrial process with rotary screen printing or continuous flatbed screen printing. The principle of this process is simple which is constituted by a screen and a squeegee. The screen has a cylindrical form and rotates around a fixed squeegee. The screen is a woven fabric made out of stainless steel or polyester covered with an emulsion layer. It is mounted to a metal frame under tension. Figure 5.12 illustrates the printing process where the screen is placed above the substrate distance by only a few millimeters. The ink is spread by moving the squeegee which moves over the screen with a sufficient pressure downward to the substrate. This allows the ink to left through the open areas of the screen behind on the substrate as the screen snaps back.

The obtained wet layer thickness is high compared to other printing techniques and the paste-like ink needs to be high viscous with thixotropic behavior. In order to avoid the clogging of the screen, the solvent should present a low volatility due to the exposition area of the ink to the environment. The principal factors of a screen are the mesh number which means mesh opening and the wire diameter. The theoretical paste volume (Vscreen) defines the wet layer thickness of the printed film. Vscreen represents the volume between the threads of the mask and the thickness of the emulsion. The volume of ink is influenced by process parameters, such as squeegee force, squeegee angle, snap-off distance, and ink rheology, summarized by the pick-out ratio, $k_p$. The dry layer thickness d can be computed by the following relation:

$$d = V_{\text{screen}}.K_P.\frac{c}{\rho}$$

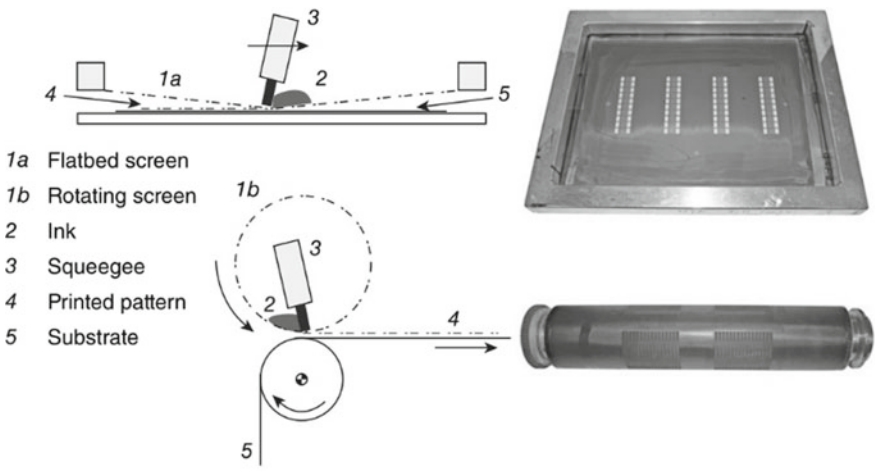


**Fig. 5.12** Principle of the flatbed and rotary screen printing process with corresponding screen

C represents the solid concentration in the ink in g/cm$^3$, and $\rho$ is the density of the dried ink material in g/cm$^3$. Screen printing is used in the industry for graphical applications, but also for printing of conductors for flexible electronics. Also, it is used to print electrodes in the silicon solar cell industry. In the field of OSCs, screen printing of the active layer polymer MEH-PPV with an adequate rheology was successfully described [88]. Many scientific researches focused on screen printing for P3HT mixtures, which show the possibility of overcoming the challenges of ink rheology and large wet thickness [65, 77, 79].

Actually, screen printing allows the deposition of conductors like PEDOT:PSS and especially for silver ink in full solution processes [19, 80]. Also, thin lines are possible, which can be used to pattern grid structures with a honeycomb-like design, as used for monolithic OSCs [82]. The silver inks can be solvent, and the influence of different types of silver ink on the performance of OSCs has been studied [49]. Other, screen printing is used to pattern the ITO layer on PET by printing etch resist and further etching, stripping, and washing of the ITO layer [17].

### *5.5.5 Gravure Printing*

Generally, in order to print graphical products with high speed (up to 20 m/s), we use the gravure printing. To get and homogenous layers with high-resolution patterning, we use the two-dimensional process and low-viscosity ink. Figure 5.13 shows the gravure printing process. The cells are filled in an ink bath or using a closed chambered doctor blade system. This is constituted by a chambered blade (doctor blade), a chromium-coated gravure cylinder, and a soft impression cylinder. To optimize the printing result, we can adjust the patterned gravure cylinder by controlling the volume (cm$^3$/m$^2$) of engraved cells, depth, width, density, and screen angle. The nip pressure allows the transfer of the ink to the substrate. The excess ink is left off just before the nip of the gravure and impression cylinder.

The pick-up volume and ink transfer rate from the cells to the substrate define the wet layer thickness. Different parameters affect the performance of the printing quality such as printing speed, pressure of the impression, and the ink rheology.

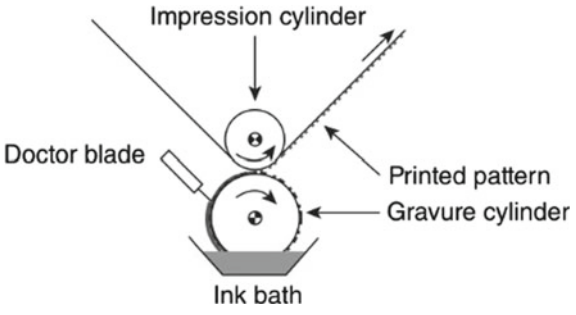


**Fig. 5.13** Gravure printing process

The deposition of materials such as PEDOT:PSS and P3HT:PCBM in organic solar cells using normal structure is recommended with gravure printing process [21, 89].

Using high concentration of the ink (150 mg/ml in o-DCB), the speed of 18 m/min is obtained in this process. For a single cell, the obtained efficiency is 2.8%, and for the module (five connected stripes), the efficiency is 1.92%.

Also, the inverted structured solar cells with three gravure printed layers ($TiO_x$, P3HT:PCBM, and PEDOT:PSS) on patterned ITO-PET substrate using a speed of 40 m/min were also manufactured with success [76]. The obtained efficiency was 0.58% with a device area of 4.5 $mm^2$.

Also, R2R gravure printing process has been used with success for organic solar cells with P3HT:PCBM active layer [90]. The substrate was paper with a ZnO/Zn/ZnO layer as electrode and the active layer was gravure printed with a speed of 12 m/min. An efficiency of 1.31% (area: 9 $mm^2$ and an illumination of 600 $W/m^2$) has been obtained using PEDOT:PSS with R2R flexo printed process.

The fabrication of organic solar cells using first the process sheet-to-sheet to show the suitability of the R2R gravure process and electrodes was evaporated. The conversion to a full R2R process where all layers are gravure printed is still possible due to the high speed and the oven length required for drying and annealing.

### *5.5.6 Flexographic Printing*

The flexographic printing is considered as R2R printing process with a speed up to 100 m/min by using a cylindrical plate carrying the printing pattern. The flexo system comprises a fountain roller which allows to fill the anilox roller with ink. The anilox roller allows a uniform thickness and equally to the printing plate cylinder. Excess ink is scraped off and it is transferred to the substrate running between the plate cylinder and impression cylinder, as shown in Fig. 5.14. A chambered doctor blade inking system can be used to avoid exposure of the ink to the atmosphere.

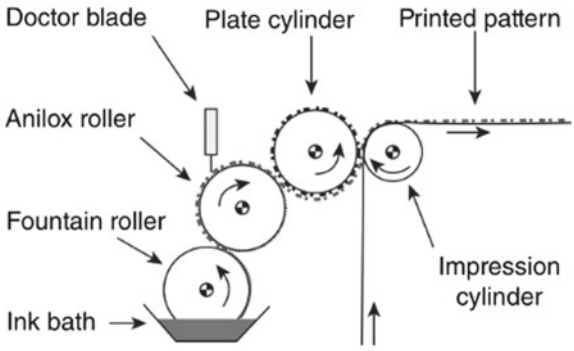


**Fig. 5.14** Illustration of the flexographic printing process

The flexographic printing has been used first for patterned PEDOT:PSS on top of P3HT:PCBM as indicated in the previous research [90].

The R2R printing of transformed PEDOT:PSS was realized with a speed of 30 m/min using an anilox cylinder (volume of 25 $cm^3/m^2$) with an efficiency of 1.31%. Flexotechnic was used for pre-wetting the surface of P3HT:PCBM with n-octanol prior to the coating of PEDOT:PSS [20]. The flexographic technic is applicable to organic photovoltaics with low volatility of the inks. Chambered doctor blade systems for the application of the ink are beneficial. It might be used for electrode production, either grids or full layer, because it can produce very thin layers. In another research work, silver grid structures (line width of 20–50 μm and distance of 0.8–2 mm) were successfully R2R printed at a speed of 5 m/min on PET [91].

### *5.5.7 Inkjet*

Generally, inkjet is used for office applications, and actually, it is used for graphical applications such as R2R industrial process. One of the most applications in the industry is the ink droplets which are generated suitable on the need.

By heating up the ink and producing a tiny bubble to allow pushing out a droplet. The piezoelectric printhead is the most used in such applications. In order to generate a pressure to push out a drop, the use of the reverse piezoelectric effect is very useful as shown in Fig. 5.15.

The ideal drops are obtained by interaction of the ink and the inkjet head. In general, the ink requires a specific voltage to drive the piezoelectric printhead. The

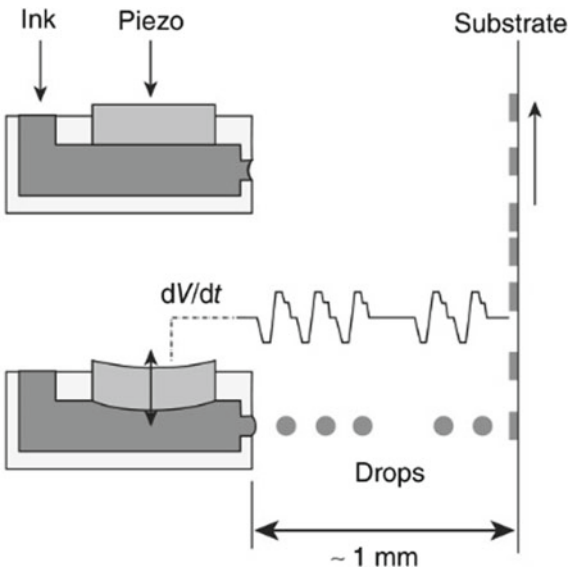


**Fig. 5.15** Inkjet printing process using the reverse piezoelectric effect for generating pressure to push out a drop

volume of the generated drop depends on the type of print head. The inkjet printing process can reach high resolution over 1200 dpi. Inkjet ink must have a low evaporation rate in order to avoid drying at the nozzle. The viscosity is an important parameter and should be lower than 30 mPa. The inks are constituted by many solvents and surfactants and the inks can either be, solvent-based, aqueous or UV curable. Many other information used for inkjet applications have been described [92–94]. Many researches on organic solar cells use inkjet process [78, 95–97]. The achieved efficiency, using inkjet process, is about 3.7% [22].

## 5.6 Conclusion

Many companies begin working to fabricate organic solar cells which present the advantage to be flexible but low efficiency. Some applications use such type of solar cells and especially in building-integrated photovoltaics. Recent researches have focused to fabricate organic solar cells with different technic such as printing process. Some of the main research areas that have already been addressed are higher efficiencies, improvements in operational stability and lifetime, multi-junction and hybrid structures, low band gap polymers and controlled morphology. New organic materials have been used in organic solar cells to get the best efficiency and good performance. Different strategies in the development of new polymers for efficient organic solar cells have been presented in many research. Solar cells efficiencies around 8% that are published are manufactured with special conditions by testing very small cell sizes. The best challenge is to achieve high efficiencies on large areas under full R2R process. But hopefully, in the near future, the strong research efforts will make this happen, so that organic solar cells can compete against other solar cell technologies.

**Acknowledgements** We would like to thank the deanship of scientific research at Islamic University (Madinah, KSA) for supporting this first (Tamayouz) program of academic year 2018/2019, research project No.: 1/40. All collaboration works are gratefully acknowledged.

## References

1. Green, M.A., et al.: Solar cell efficiency tables (Version 38). Prog. Photovoltaics Res. Appl. **19**(5), 565–572 (2011)
2. Tang, C.: Two-layer organic photovoltaic cell. Appl. Phys. Lett. **48**, 183 (1986)
3. Sariciftci, N.S., et al.: Observation of a photoinduced electron transfer from a conducting polymer (MEHPPV) onto C60. Synth. Met. **56**(2–3), 3125–3130 (1993)
4. Spanggaard, H., Krebs, F.C.: A brief history of the development of organic and polymeric photovoltaics. Sol. Energy Mater. Sol. Cells **83**(2–3), 125–146 (2004)
5. Brabec, C.J., Sariciftci, N.S., Hummelen, J.: Plastic solar cells. Adv. Func. Mater. **11**(1), 15–26 (2001)

6. Coakley, K., McGehee, M.D.: Conjugated polymer photovoltaic cells. Chem. Mater. **16**(23), 4533–4542 (2004)
7. Hoppe, H., Sariciftci, N.S.: Organic solar cells: an overview. J Mater Researd **19**(7), 1924–1945 (2004)
8. Dennler, G., Sariciftci, N.S.: Flexible conjugated polymer-based plastic solar cells: from basics to applications. Proc. IEEE **93**(8), 1429–1439 (2005)
9. Brabec, C.J., Dyakonov, V., Scherf, U.: Organic Photovoltaics, Wiley-VCH (2008)
10. Krebs, F.C.: Polymer Photovoltaics: A Practical Approach. SPIE Publications (2008)
11. Thompson, B., Frechet, J.M.J.: Polymer—fullerene composite solarcells. Angew. Chem. Int. Ed. **47**(1), 58–77 (2008)
12. Deibel, C., Dyakonov, V.: Polymer–fullerene bulk-heterojunction solar cells. Rep. Prog. Phys. **73**, 096401 (2010)
13. Helgesen, M., Søndergaard, R., Krebs, F.C.: Advanced materials and processes for polymer solar cell devices. J. Mater. Chem. **20**(1), 36–60 (2010)
14. Po, R., Maggini, M., Camaioni, N.: Polymer solar cells: recent approaches and achievements. J. Phys. Chem. C **114**(2), 695–706 (2010)
15. Servaites, J.D., Ratner, M.A., Marks, T.J.: Organic solar cells: a new look at traditional models. Energy Environ. Sci. **4**, 4410–4422 (2011)
16. Zhang, F., et al.: Recent development of the inverted configuration organic solar cells. Sol. Energy Mater. Sol. Cells **95**(7), 1785–1799 (2011)
17. Krebs, F.C.: Fabrication and processing of polymer solar cells: a review of printing and coating techniques. Sol. Energy Mater. Sol. Cells **93**(4), 394–412 (2009)
18. Søndergaard, R., et al.: Roll-to-roll fabrication of polymer solar cells. Mater. Today **15**(1–2), 36–49 (2012)
19. Krebs, F.C., Tromholt, T., Jørgensen, M.: Upscaling of polymer solar cell fabrication using full roll-to-roll processing. Nanoscale **2**(6), 873–886 (2010)
20. Krebs, F.C.: All solution roll-to-roll processed polymer solar cells free from indium-tin-oxide and vacuum coating steps. Org. Electron. **10**(5), 761–768 (2009)
21. Kopola, P., et al.: Gravure printed flexible organic photovoltaic modules. Sol. Energy Mater. Sol. Cells **95**(5), 1344–1347 (2011)
22. Eom, S.H., et al.: High efficiency polymer solar cells via sequential inkjet-printing of PEDOT:PSS and P3HT:PCBM inks with additives. Org. Electron. **11**(9), 1516–1522 (2010)
23. Nielsen, T., et al.: Business, market and intellectual property analysis of polymer solar cells. Sol. Energy Mater. Sol. Cells **94**(10), 1553–1571 (2010)
24. Koster, L., Mihailetchi, V., Blom, P.W.M.: Ultimate efficiency of polymer/fullerene bulk heterojunction solar cells. Appl. Phys. Lett. **88**, 093511 (2006)
25. Scharber, M.C., et al.: Design rules for donors in bulk-heterojunction solar cells—towards 10% energy-conversion efficiency. Adv. Mater. **18**(6), 789–794 (2006)
26. Krebs, F.C., Spanggaard, H.: Significant improvement of polymer solar cell stability. Chem. Mater. **17**(21), 5235–5237 (2005)
27. Hauch, J., et al.: Flexible organic P3HT: PCBM bulk-heterojunction modules with more than 1 year outdoor lifetime. Sol. Energy Mater. Sol. Cells **92**(7), 727–731 (2008)
28. Zimmermann, B., Würfel, U., Niggemann, M.: Longterm stability of efficient inverted P3HT: PCBM solar cells. Sol. Energy Mater. Sol. Cells **93**(4), 491–496 (2009)
29. Voroshazi, E., et al.: Long-term operational lifetime and degradation analysis of P3HT:PCBM photovoltaic cells. Sol. Energy Mater. Sol. Cells **95**(5), 1303–1307 (2011)
30. Basics of OSC: Organic solar cells, [Online]. Available: https://www.iapp.de/iapp/agruppen/osol/?Research:Organic_Solar_Cells:Basics_of_OSC
31. Dam, H.F., Larsen-Olsen, T.T.: How do polymer solar cells work [Online]. Available: http://plasticphotovoltaics.org/lc/lc-polymersolarcells/lc-how.html
32. Blom, P.W.M., et al.: Device physics of polymer: fullerene bulk heterojunction solar cells. Adv. Mater. **19**(12), 1551–1566 (2007)
33. Halls, J., et al.: Exciton diffusion and dissociation in a poly (p-phenylenevi-nylene)/C60 heterojunction photovoltaic cell. Appl. Phys. Lett. **68**, 3120 (1996)

34. Haugeneder, A., et al.: Exciton diffusion and dissociation in conjugated polymer/fullerene blends and heterostructures. Phys. Rev. B **59**(23), 15346 (1999)
35. Pettersson, L.A.A., Roman, L.S., Inganäs, O.: Modeling photocurrent action spectra of photovoltaic devices based on organic thin films. J. Appl. Phys. **86**, 487 (1999)
36. Piris, J., et al.: Photogeneration and ultrafast dynamics of excitons and charges in P3HT/PCBM blends. J. Phys. Chem. C **113**(32), 14500–14506 (2009)
37. Li, G., et al.: High-efficiency solution processable polymer photovoltaic cells by self-organization of polymer blends. Nat. Mater. **4**, 864–868 (2005)
38. Ma, W., et al.: Thermally stable, efficient polymer solar cells with nanoscale control of the interpenetrating network morphology. Adv. Func. Mater. **15**(10), 1617–1622 (2005)
39. Espinosa, N., et al.: A life cycle analysis of polymer solar cell modules prepared using roll-to-roll methods under ambient conditions. Sol. Energy Mater. Sol. Cells **95**(5), 1293–1302 (2011)
40. Galagan, Y., Rubingh, J.M., et al.: ITO-free flexible organic solar cells with printed current collecting grids. Solar Energy Mater. Solar Cells, **95**(5), 1339–1343 (2011a)
41. Po, R., et al.: The role of buffer layers in polymer solar cells. Energy Environ. Sci. **4**(2), 285–310 (2011)
42. Søndergaard, R., et al.: Fabrication of polymer solar cells using aqueous processing for all layers including the metal back electrode. Adv. Energy Mater. **1**(1), 68–71 (2010)
43. Gilot, J., et al.: The use of ZnO as optical spacer in polymer solar cells: theoretical and experimental study. Appl. Phys. Lett. **91**(11), 113520–4 (2007)
44. Hayakawa, A., et al.: High performance polythiophene/fullerene bulk-hetero-junction solar cell with a $TiO_x$ hole blocking layer. Appl. Phys. Lett. **90**(16), 163517–4 (2007)
45. Lee, K., et al.: Air-stable polymer electronic devices. Adv. Mater. **19**(18), 2445–2449 (2007)
46. Huang, J.-S., Chou, C.-Y., Lin, C.-F.: Efficient and air-stable polymer photo-voltaic devices with $WO_3$-$V_2O_5$ mixed oxides as anodic modification. Electron Device Lett. IEEE **31**(4), 332–334 (2010)
47. Dupont, S.R., et al.: Interlayer adhesion in roll-to-roll processed flexible inverted polymer solar cells. Sol. Energy Mater. Sol. Cells **97**, 171–175 (2012)
48. Brabec, C.J., et al.: Effect of LiF/metal electrodes on the performance of plastic solar cells. Appl. Phys. Lett. **80**(7), 1288 (2002)
49. Krebs, F.C., Søndergaard, R., Jørgensen, M.: Printed metal back electrodes for R2R fabricated polymer solar cells studied using the LBIC technique. Sol. Energy Mater. Sol. Cells **95**(5), 1348–1353 (2011)
50. Dennler, G., Lungenschmied, C., Neugebauer, H.: Flexible, conjugated polymer-fullerene-based bulk-heterojunction solar cells: Basics, encapsulation and integration. J. Mater. Res. **20**(12), 3224–3233 (2005)
51. Lungenschmied, C., Dennler, G., Neugebauer, H.: Flexible, long-lived, large-area, organic solar cells. Sol. Energy Mater. Sol. Cells **91**(5), 379–384 (2007)
52. Tanenbaum, D.M., et al.: Edge sealing for low cost stability enhancement of roll-to-roll processed flexible polymer solar cell modules. Sol. Energy Mater. Sol. Cells **97**, 157–163 (2012)
53. Yu, G., et al.: Polymer photovoltaic cells: enhanced efficiencies via a network of internal donor-acceptor heterojunctions. Science **270**(5243), 1789–1791 (1995)
54. Bundgaard, E., Krebs, F.C.: Low band gap polymers for organic photovoltaics. Sol. Energy Mater. Sol. Cells **91**(11), 954–985 (2007)
55. Boland, P., Lee, K., Namkoong, G.: Device optimization in PCPDTBT:PCBM plastic solar cells. Sol. Energy Mater. Sol. Cells **94**(5), 915–920 (2010)
56. Kumar, P., Chand, S.: Recent progress and future aspects of organic solar cells. Prog. Photovoltaics Res. Appl. **20**, 377–415 (2011)
57. Dang, M.T., et al.: Polymeric solar cells based on P3HT:PCBM role of the casting solvent. Sol. Energy Mater. Sol. Cells **95**(12), 3408–3418 (2011)
58. Dennler, G., Scharber, M.C., Brabec, C.J.: Polymer-fullerene bulk-hetero-junction solar cells. Adv. Mater. **21**(13), 1323–1338 (2009)

59. Padinger, F., Rittberger, R., Sariciftci, N.S.: Effects of postproduction treatment on plastic solar cells. Adv. Func. Mater. **13**(1), 85–88 (2003)
60. Benanti, T., Venkataraman, D.: Organic solar cells: an overview focusing on active layer morphology. Photosynth. Res. **87**(1), 73–81 (2006)
61. Chirvase, D., Parisi, J., Hummelen, J.: Influence of nanomorphology on the photovoltaic action of polymer–fullerene composites. Nanotechnology **15**, 1317–1323 (2004)
62. Zhao, Y., et al.: Solvent-vapor treatment induced performance enhancement of poly (3-hexylthiophene): methanofullerene bulk-heterojunction photovoltaic cells. Appl. Phys. Lett. **90**, 043504 (2007)
63. Gevorgyan, S.A., Krebs, F.C.: Bulk heterojunctions based on nativepolythiophene. Chem. Mater. **20**(13), 4386–4390 (2008)
64. Petersen, M., Gevorgyan, S.A., Krebs, F.C.: Thermocleavable low band gap polymers and solar cells therefrom with remarkable stability toward oxygen. Macromolecules **41**(23), 8986–8994 (2008)
65. Jørgensen, M., Hagemann, O., Alstrup, J.: Thermo-cleavable solvents for printing conjugated polymers: application in polymer solar cells. Sol. Energy Mater. Sol. Cells **93**(4), 413–421 (2009)
66. Sista, S., et al.: Tandem polymer photovoltaic cells—current status, challenges and future outlook. Energy Environ. Sci. **4**(5), 1606 (2011)
67. Weickert, J., et al.: Nanostructured organic and hybrid solar cells. Adv. Mater. **23**(16), 1810–1828 (2011)
68. Peumans, P., Yakimov, A., Forrest, S.R.: Small molecular weight organic thin-film photodetectors and solar cells. J. Appl. Phys. **93**(7), 3693–3723 (2003)
69. Rand, B.P., et al.: Solar cells utilizing small molecular weight organic semiconductors. Prog. Photovoltaics Res. Appl. **15**(8), 659–676 (2007)
70. Maennig, B., et al.: Organic p-i-n solar cells. Appl. Phys. A Mater. Sci. Process. **79**(1), 1–14 (2004)
71. Riede, M., et al.: Small-molecule solar cells—status and perspectives. Nanotechnology, **19**(42), 424001 (2008)
72. Yoo, S., Domercq, B., Kippelen, B.: Efficient thin-film organic solar cells based on pentacene/C60 heterojunctions. Appl. Phys. Lett. **85**(22), 5427 (2004)
73. Schulze, K., et al.: Efficient vacuum-deposited organic solar cells based on a new low-bandgap oligothiophene and fullerene C60. Adv. Mater. **18**(21), 2872–2875 (2006)
74. Riede, M., et al.: Efficient organic tandem solar cells based on small molecules. Adv. Func. Mater. **21**(16), 3019–3028 (2011)
75. Zhang, L., et al.: Triisopropylsilylethynyl-functionalized dibenzo[def, mno]chrysene: a solution-processed small molecule for bulk heterojunction solar cells. J. Mater. Chem. **22**(10), 4266 (2012)
76. Voigt, M.M., et al.: Gravure printing for three subsequent solar cell layers of inverted structures on flexible substrates. Sol. Energy Mater. Sol. Cells **95**, 731–734 (2011)
77. Zhang, B., Chae, H., Cho, S.: Screen-printed polymer: fullerene bulk-heterojunction solar cells. Jap. J. Appl. Phys. **48**(2), 020208–1–020208–3 (2009)
78. Lange, A., et al.: A new approach to the solvent system for inkjet-printed P3HT:PCBM solar cells and its use in devices with printed passive and active layers. Sol. Energy Mater. Sol. Cells **94**(10), 1816–1821 (2010)
79. Krebs, F.C., Jørgensen, M., Norrman, K., Hagemann, O., et al.: A complete process for production of flexible large area polymer solar cells entirely using screen printing—first public demonstration. Sol. Energy Mater. Sol. Cells **93**(4), 422–441 (2009)
80. Galagan, Y., Rubingh, J.-E., et al.: ITO-free flexible organic solar cells with printed current collecting grids. Solar Energy Mater. Solar Cells, **95**(5), 1339–1343 (2011a)
81. Hoppe, H., Seeland, M., Muhsin, B.: Optimal geometric design of monolithic thin-film solar modules: architecture of polymer solar cells. Sol. Energy Mater. Sol. Cells **97**, 119–126 (2012)
82. Manceau, M., et al.: ITO-free flexible polymer solar cells: from small model devices to roll-to-roll processed large modules. Org. Electron. **12**(4), 566–574 (2011)

83. Gutoff, E.B., Cohen, E.D.: Coating and drying defects, 2nd edn. Wiley, Hoboken, NJ (2006)
84. Tracton, A.A.: Coatings Technology. CRC Press, Boca Raton, FL (2007)
85. Kipphan, H.: Handbook of print media. Springer Verlag, Berlin, Heidelberg, New York (2001)
86. Krebs, F.C., Gevorgyan, S.A., Alstrup, J.: A roll-to-roll process to flexible polymer solar cells: model studies, manufacture and operational stability studies. J. Mater. Chem. **19**(30), 5442–5451 (2009)
87. Alstrup, J., et al.: Ultra fast and parsimonious materials screening for polymer solar cells using differentially pumped slot-die coating. ACS Appl. Mater. Interfaces. **10**(2), 2819–2827 (2010)
88. Krebs, F.C., et al.: Large area plastic solar cell modules. Mater. Sci. Eng., B **138**(2), 106–111 (2007)
89. Kopola, P., et al.: High efficient plastic solar cells fabricated with a high-throughput gravure printing method. Sol. Energy Mater. Sol. Cells **94**(10), 1673–1680 (2010)
90. Hübler, A.C., et al.: Printed paper photovoltaic cells. Adv Energy Mater **1**(6), 1018–1022 (2011)
91. Deganello, D., et al.: Patterning of micro-scale conductive networks using reel-to-reel flexographic printing. Thin Solid Films **518**(21), 6113–6116 (2010)
92. Derby, B.: Inkjet printing of functional and structural materials: fluid property requirements, feature stability, and resolution. Annu. Rev. Mater. Res. **40**, 395–414 (2010)
93. Pond, S.F.: Inkjet technology and product development strategies. Torrey Pines Res, Carlsbad (2000)
94. Magdassi, S.: The Chemistry of Inkjet Inks. World Scientific Publishing, Singapore (2010)
95. Hoth, C.N., et al.: High photovoltaic performance of inkjet printedpolymer: fullerene blends. Adv. Mater. **19**(22), 3973–3978 (2007)
96. Hoth, C.N., et al.: Printing highly efficient organic solar cells. Nano Lett. **8**(9), 2806–2813 (2008)
97. Kim, J.-M., et al.: Polymer based organic solar cells using ink-jet printed active layers. Appl. Phys. Lett. **92**, 033306 (2008)